Available online at www.sciencedirect.com
SCIENCE DIRECT®
Bioorganic & Medicinal Chemistry 14 (2006) 4923–4932
Bioorganic & Medicinal Chemistry

The application of a 3D-QSAR (*auto*MEP/PLS) approach as an efficient pharmacodynamic-driven filtering method for small-sized virtual library: Application to a lead optimization of a human A_3 adenosine receptor antagonist

Stefano Moro,[a,*] Magdalena Bacilieri,[a] Barbara Cacciari,[b] Chiara Bolcato,[c] Claudia Cusan,[c] Giorgia Pastorin,[c] Karl-Norbert Klotz[d] and Giampiero Spalluto[c,*]

[a]*Molecular Modeling Section, Dipartimento di Scienze Farmaceutiche, Università di Padova, via Marzolo 5, I-35131 Padova, Italy*
[b]*Dipartimento di Scienze Farmaceutiche, Università degli Studi di Ferrara, Via Fossato di Mortara 17-19, I-44100 Ferrara, Italy*
[c]*Dipartimento di Scienze Farmaceutiche, Università degli Studi di Trieste, Piazzale Europa 1, I-34127 Trieste, Italy*
[d]*Institut für Pharmakologie und Toxikologie, Universität Würzburg, Versbacher Str. 9, D-97078 Würzburg, Germany*

Received 5 January 2006; revised 2 March 2006; accepted 8 March 2006
Available online 29 March 2006

Abstract—We have recently reported that the combination of molecular electrostatic potential (MEP) surface properties (autocorrelation vectors) with the conventional partial least squares (PLS) analysis can be used to produce a robust ligand-based 3D structure–activity relationship (*auto*MEP/PLS) for the prediction of the human A_3 receptor antagonist activities. Here, we present the application of the 3D-QSAR (*auto*MEP/PLS) approach as an efficient and alternative pharmacodynamic filtering method for small-sized virtual library. For this purpose, a small-sized combinatorial library (841 compounds) was derived from the scaffold of the known human A_3 antagonist pyrazolo-triazolo-pyrimidines. The most interesting analogues were further prioritized for synthesis and pharmacological characterization. Remarkably, we have found that all the newly synthetized compounds are correctly predicted as potent human A_3 antagonists. In particular, two of them are correctly predicted as sub-nanomolar inhibitors of the human A_3 receptor.

1. Introduction

The generation of novel structures amenable to rapid and efficient lead optimization comprises an emerging strategy for success in modern drug discovery.[1] Small molecule libraries of sufficient size and diversity to increase the chances of discovery of novel structures make the high-throughput synthesis approach the method of choice for lead generation.[2] However, to provide realistic means for rapidly scanning the combinatorial chemistry libraries now available for high-throughput screening (HTS), it is essential to establish computational virtual ligand screening (VLS) techniques to rapidly identify out of a large library all possible active compounds against a particular protein target.[3–5] All filtering strategies able to select chemical compounds based on their target complementarity can be defined as pharmacodynamic-driven filtering methods. Pharmacophore-based or high-throughput docking filtering are two examples of very well-documented pharmacodynamic-driven filtering methods.[6–8] Of course, in tandem with pharmacodynamic-driven filtering methods, drug likeness-based or other pharmacokinetics filtering strategies can be adopted during library design or library screening. Several examples of drug likeness or pharmacokinetics-based filtering have been already reported.[4,9–11]

The principal aim of the present work was the investigation of a new alternative pharmacodynamic-driven filtering method. In fact, we have recently reported that the combination of molecular electrostatic potential (MEP) surface properties (autocorrelation vectors) with the conventional partial least squares (PLS) analysis can

Keywords: GPCR; A_3 adenosine receptor antagonist; 3D-QSAR; Molecular modeling.
* Corresponding authors. Tel.: +39 049 827 5704; fax: +39 049 827 5366; e-mail: stefano.moro@unipd.it

0968-0896/$ - see front matter © 2006 Elsevier Ltd. All rights reserved.
doi:10.1016/j.bmc.2006.03.010

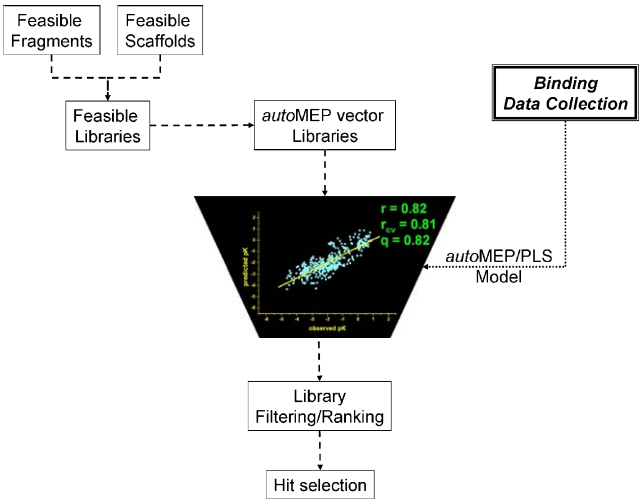

Figure 1. Flow chart describing our pharmacodynamic-driven (*auto*MEP/PLS) filtering method for small-size virtual library.

be used to produce a robust ligand-based 3D structure–activity relationship (*auto*MEP/PLS) for the prediction of the human A_3 adenosine receptor (A_3R) antagonist activities.[12,13] A_3 adenosine receptors belong to the adenosine receptors (ARs) family of GPCRs, which consists of four distinct subtypes: A_1, A_{2A}, A_{2B}, and A_3. ARs are ubiquitously expressed in the human body.[14–16] The human A_3R (h_A_3R), which is the most recently identified adenosine receptor, is implicated in a variety of important physiopathological processes.[14–16]

Herein, we present the application of 3D-QSAR (*auto*MEP/PLS) approach as efficient and alternative pharmacodynamic-driven filtering method for small-size virtual library (see Fig. 1). For this propose, a small-sized combinatorial library (841 compounds) was derived from the scaffold of the known human A_3 antagonist pyrazolo-triazolo-pyrimidines.[12,17] The most interesting analogues were further prioritized for synthesis and pharmacological characterization. Remarkably, we found that all the newly synthetized compounds are correctly predicted as potent human A_3 antagonists. In particular, two of them are correctly predicted as sub-nanomolar inhibitors of the human A_3 receptor.

2. Results and discussion

2.1. Setup of a pyrazolo-triazolo-pyrimidine focused library

As already described pyrazolo-triazolo-pyrimidines bearing different substitutions at the N^5 and N^8 positions have been characterized as potent and selective human A_3 adenosine receptor antagonists.[12,13,17,18] To validate our *auto*MEP/PLS library filtering approach, 29 molecular fragments were assembled according to the combinatorial scheme described in Table 1.

To freely explore the topological space around both N^5 and N^8 positions, and consequently to rigorously validate our virtual library filtering approach, all 29 functional groups were finally selected only for their synthetic feasibility. Moreover, most of the 29 molecular fragments represent new substitutions at both N^5 and N^8 positions compared to all the already published pyrazolo-triazolo-pyrimidines.[12,13,17,18] Indeed, 841 structures were altogether generated to be part of the new virtual library. Following our recently reported methodology,[12,13] autocorrelation MEP vectors have been calculated for each chemical compound of our virtual library (see Section 3 for details). In fact, autocorrelation vector descriptors represent a chemical structure with a vector of fixed length independent of the size of the molecule. Since only internal coordinates (topological or spatial distances of atom pairs or pairs of points on the molecular surface) are taken into account, the resulting descriptors are also independent from the orientation of the molecules in space (translation and rotation invariant). Therefore, no pre-processing alignment of the molecules in a dataset should be necessary.[19,20]

2.2. *auto*MEP/PLS library filtering approach

As mentioned above, we have reported that the combination of molecular electrostatic potential (MEP) surface properties with the conventional partial least squares (PLS) analysis can be used for the prediction of the human A_3 receptor antagonist activities (*auto*MEP/PLS approach).[12,13] Starting from 358 structurally diverse human A_3 receptor antagonists, a robust quantitative model has been obtained ($r = 0.82$, $r_{cv} = 0.81$, $q = 0.82$).[13] Considering the distinct characteristics of our *auto*MEP/PLS strategy, we hypothesized that this method might be useful for hit identification and/or lead optimization processes. In fact, the transformation of MEP surfaces into autocorrelation vectors produces a unique fingerprint of each molecule under consideration. Each fingerprint can be used as input for our *auto*MEP/PLS model, providing the predicted activity as output. In other words, we can consider the application of *auto*MEP/PLS model strategy as a potential new pharmacodynamic-driven filtering method for chemical libraries.

Following this strategy, after the binding affinity prediction step we have inspected the compounds predicted as more active (~100 molecules) with a spectrum of predicted activity in the range of 0.1–4.0 nM. We have carefully analyzed physicochemical properties (such as lipophilicity, water solubility, and chemical stability) and synthetic feasibility of all these top library candidates, and on the basis of their best compromise, we selected nine analogues which were further prioritized for synthesis and pharmacological characterization. All compounds were predicted as potent human A_3 adenosine antagonists as shown in Table 2 and Figure 2. Impressively, derivatives **2** and **4** are correctly predicted as sub-nanomolar inhibitors of the human A_3 receptor. However, some of them lose their specificity versus the human A_3 receptor. In fact, derivatives **1** and **3** are quite potent as human A_{2A} receptor antagonist. To specifically address the selectivity profile of new adenosine antagonists, we are implementing a multiple *auto*MEP/PLS model

Table 1.

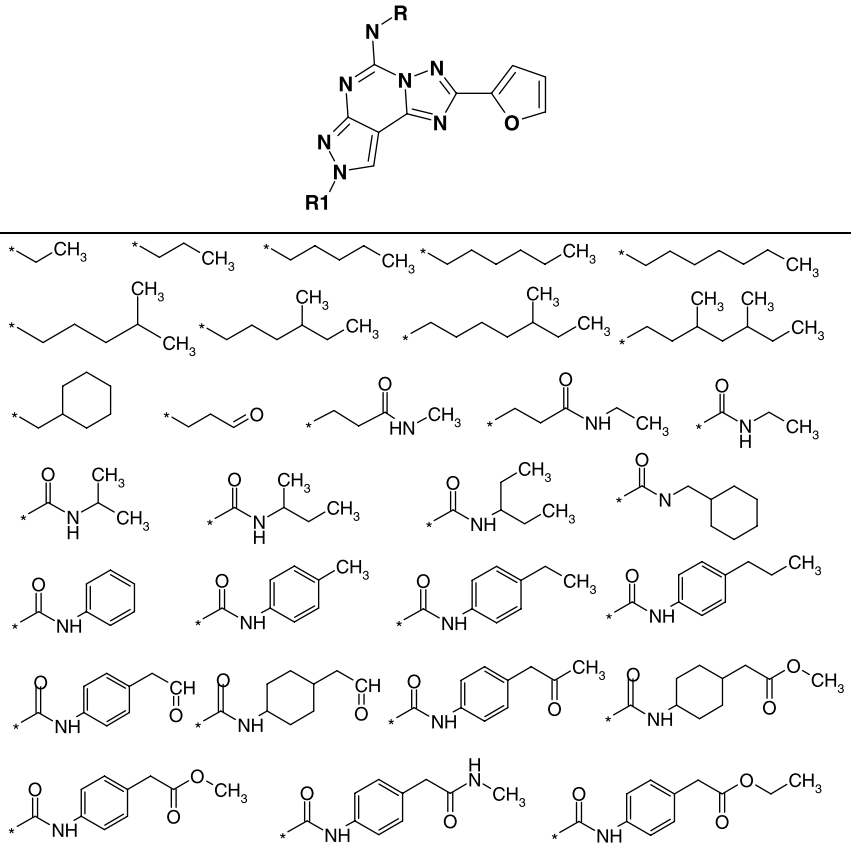

in which we will be able to predict, simultaneously, the receptor binding affinity versus all adenosine receptor subtypes.

Indeed, it is important to point out that the main application of our *auto*MEP/PLS approach is to identify new potent human A_3 adenosine antagonists browsing a large collection of chemical compounds and not specifically searching for the precise quantitative value of their activities.

Interestingly, all the selected compounds bear two hydrophobic fragments at both N^5 and N^8 positions confirming our already documented structure–activity relationships.[16,17] Furthermore, to better describe the ligand–receptor complementarity a molecular docking study has been performed.

2.3. Docking of the selected human A_3 antagonist candidates

In order to further investigate if all selected human A_3 antagonist candidates can also fit into the receptor binding cavity, a molecular docking study has been carried out. Using a high-throughput docking strategy, we have recently analyzed more than 300 known human A_3 antagonists in the corresponding putative ligand binding site.[15–17] A consensus binding motif among all known antagonists has been found, and a novel 'Y-shaped' 3D-pharmacophore model has been proposed.[16,17] After molecular docking study, we have confirmed that all the selected compounds nicely fit into our 'Y-shaped' pharmacophore model, as shown in Figure 3.

In more detail, our pharmacophore model fits in a complementary fashion inside the TM region, occupying the upper region of the helical bundle. His95 (TM3) and Ser247 (TM6) appear to be very critical for the recognition of the antagonist structures. In fact, a major structural difference between the hypothetical binding sites in these receptor subtypes is that the A_3 receptor does not contain the histidine residue in TM6 common to A_1 (His251 in human A_1) and A_2 (His250 in human A_{2A}) receptors. This histidine has been shown to participate in both agonist and antagonist binding to A_{2A} receptors. In the A_3 receptor this histidine in TM6 is replaced with a serine residue (Ser247 in human A_3). Another strong hydrogen bonding interaction is possible with Asn250 (TM6). This asparagine residue, conserved among all adenosine receptor subtypes, was found to be important for ligand binding. An important and peculiar hydrophobic pocket delimited by non-polar amino acids, Leu90 (TM3), Leu246 (TM6), and Ile268 (TM7), is also present in our binding site model. Another important and highly conserved region, probably stabilized by π–π interactions, is located between Phe168 (EL2) and Phe182 (TM5). This region seems to be another important pharmacophore feature of our binding motif.

Table 2.

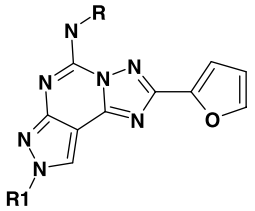

Compound	R	R^1	hA_1 (K_i, nM)	hA_{2A} (K_i, nM)	hA_{2B} (IC_{50}, nM)	hA_3 (K_i, nM)	pred_hA_3 (K_i, nM)
CB1	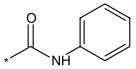		310 (295–327)	27.7 (13.3–57.8)	3440 (2880–4110)	1.80 (0.88–3.68)	0.92
1	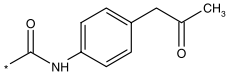	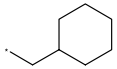	71.8 (44.1–117).	6.80 (3.57–13.0)	7020 (6070–8120)	42.3 (14–127)	1.77
2	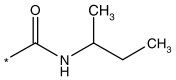		376 (342–414)	559 (500–624)	>30,000	0.53 (0.47–0.59)	0.84
3	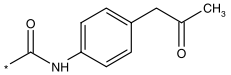	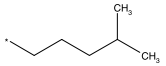	−137 (72.0–262)	−24.8 (11.1–55.2)	−13,000 (10,200–16,600)	68.8 (33.9–140)	1.79
4	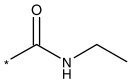	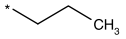	77.2 (64.1–93)	223 (208–238)	2810 (1930–4130)	0.60 (0.53–0.68)	0.52
5	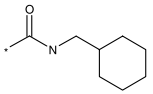	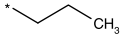	13.8 (10.4–18.2)	258 (210–318)	3440 (1300–9100)	3.53 (2.09–5.99)	4.33
6	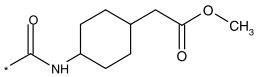	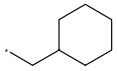	52.5 (31.2–88.4)	5.74 (4.27–7.72)	8940 (8430–9490)	164 (82.1–326)	1.30
7	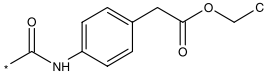	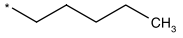	54.7 (35.3–84.9)	4.77 (3.04–7.49)	9740 (7.0–12,600)	18 (14.2–22.8)	1.88
8	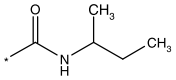		576 (551–602)	300 (253–356)	>100,000	5.33 (4.48–6.35)	5.97
9	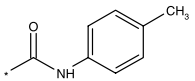		34.7 (27.4–43.9)	3.72 (3.07–4.51)	2910 (1310–6460)	44.4 (35.9–54.9)	5.43

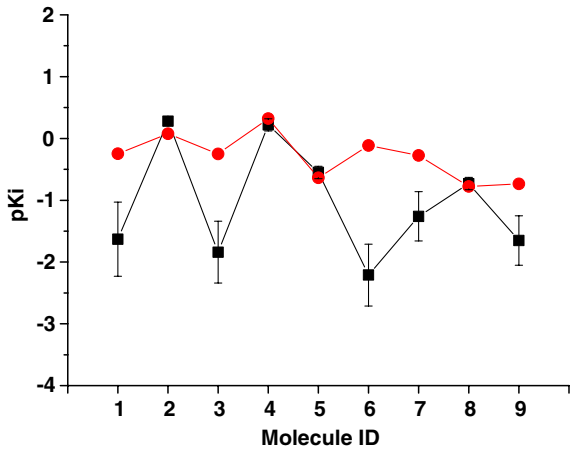

Figure 2. Comparison of experimental pK_i values (■) with those predicted by *auto*MEP/PLS QSAR model (●).

The amino acids corresponding to Leu90 and Phe182 in the human A_{2A} receptor were found to be essential for the binding of both agonists and antagonists. The last crucial pharmacophore region is mostly hydrophobic and characterized by three non-polar amino acids: Ile98 (TM3), Ile186 (TM5), and Leu244 (TM6).

2.4. Synthesis of the selected human A_3 antagonist candidates

Compounds **1**–**9** were prepared following the general synthetic strategy summarized in Scheme 1. They were synthesized according to a well-known procedure for the synthesis of the pyrazolo[4,3-*e*]-1,2,4-triazolo[1,5-*c*]pyrimidines, previously reported.[17,21,22]

Alkylation of 5-amino-4-cyano-pyrazole **10** with the appropriate alkyl halide in dry dimethylformamide led to an approximately 1:4 mixture of the N^1 and N^2 regioisomers (**11**–**13**) as an inseparable mixture, used for the following steps without any further purification.

Pyrazoles (**11**–**13**) were reacted with 2-furoic in diphenyl ether at 260 °C to yield the aminotriazoles **14**–**16**, which were in turn converted into the 5-amino-8-(substituted)-2-(2-furyl) pyrazolo[4,3-*e*]-1,2,4-triazolo-[1,5-*c*]pyrimidine derivatives by reaction with cyanamide in the presence of *p*-toluen sulfonic acid. After separation of N^7 (minor product) and N^8 (major product) regioisomers by flash chromatography, the desired compounds **17**–**19** were obtained in good overall yield. Final compounds **1**–**9** were obtained by reaction of amino compounds **17**–**22** with the appropriate isocyanate (**23**–**29**) in dioxane at reflux. When not commercially available, isocyanate was prepared by the corresponding anilines by treatment with trichloromethylchloroformate, as described in the literature.[23]

2.5. Final remarks

Virtual screening of chemical databases and virtual libraries is now a well-established method to identify new hit candidates in the drug discovery process. In this paper, we present the application of 3D-QSAR (*auto*-MEP/PLS) approach as an efficient and alternative pharmacodynamic filtering method for small-size virtual library (841 compounds) derived from the scaffold of the known human A_3 antagonist pyrazolo-triazolo-pyrimidines. The results shown here are encouraging as all selected compounds show high potency versus the human A_3 receptor maintaining, in case of compounds **2** and **4** an excellent selectivity versus all other adenosine receptor subtypes. However, we are running an intense virtual screening program to validate the capability of the presented *auto*MEP/PLS model to discover novel

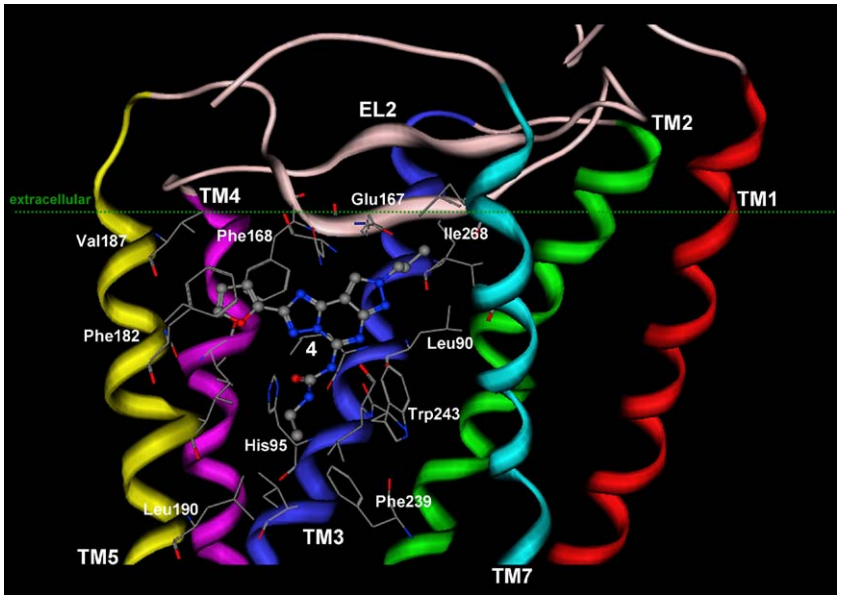

Figure 3. General topology of the human A_3 adenosine receptor obtained using a rhodopsin-based homology modeling where the best docked conformation of derivative **4** is shown (see Section 3 for details). The sidechains of some crucial important residues in proximity (⩽5 Å) to the antagonist binding cavity are highlighted and labeled: Leu90 (TM3), His95 (TM3), Phe182 (TM5), Ile186 (TM5), Trp243 (TM6), Ser247 (TM6), Asn250 (TM6), Ser271 (TM7), His272 (TM7), and Ser275 (TM7). To clarify the TM cavity viewing, TM6 has been voluntarily omitted.

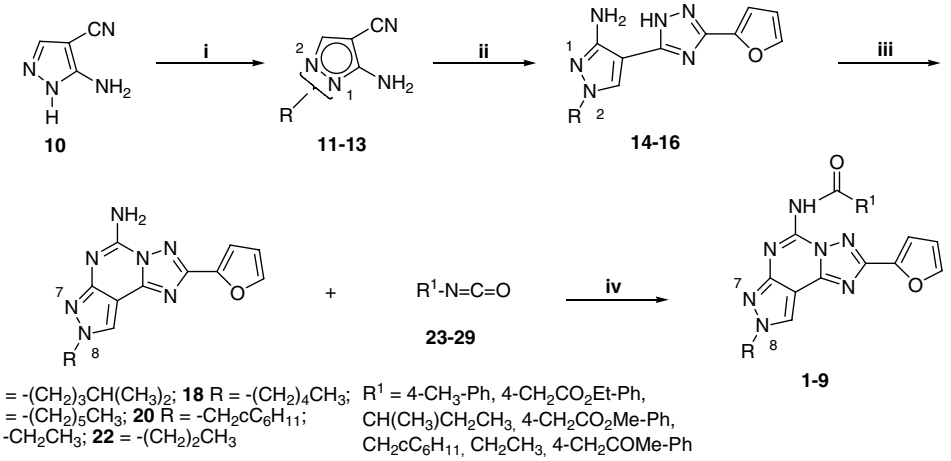

Scheme 1. Reagents and conditions: (i) NaH, DMF, RX; (ii) 2-furoic hydrazide, Ph_2O, 260 °C; (iii) NH_2CN, 1-methyl-2-pyrolidone, pTsOH, 140 °C, then flash chromatography; (iv) dioxane reflux, 18 h. For compounds **20**–**22**, see Refs. 2 and 3.

chemically diverse A_3 antagonists using large (available compounds or virtual) chemical libraries.

3. Experimental

3.1. Chemistry

3.1.1. General. Reactions were routinely monitored by thin-layer chromatography (TLC) on silica gel (precoated F_{254} Merck plates) and products visualized with iodine or potassium permanganate solution. Infrared spectra (IR) were measured on a Perkin-Elmer 257 instrument. ^{1}H NMR were determined in $CDCl_3$ or DMSO-d_6 solutions with a Bruker AC 200 spectrometer, peak positions are given in parts per million (δ) downfield from tetramethylsilane as internal standard, and J values are given in hertz. Light petroleum ether refers to the fractions boiling at 40–60 °C. Melting points were determined on a Buchi-Tottoli instrument and are uncorrected. Chromatographies were performed using Merck 60-200 mesh silica gel. All reported products showed IR and ^{1}H NMR spectra in agreement with the assigned structures. Organic solutions were dried over anhydrous magnesium sulfate. Elemental analyses were performed by the microanalytical laboratory of Dipartimento di Chimica, University of Trieste, and they were within ±0.4% of the theoretical values for C, H, and N.

3.1.2. General procedures for the preparation of 8-alkyl-2-(2-furyl)-pyrazolo[4,3-*e*]1,2,4-triazolo[1,5-*c*]pyrimidines (17–19). A solution of **10** (10 mmol) in 40 mL of DMF cooled to 0 °C was treated with NaH (60% in oil, 12 mmol) in several portions over 10 min. After 45 min, the appropriate alkyl halide (12 mmol) was added and the reaction mixture was allowed to warm to 25 °C and stirred for 3–5 h (TLC–EtOAc 1:1). The reaction was quenched by addition of H_2O (80 mL), and the aqueous layer was extracted with EtOAc (5× 25 mL). The organic layers were recombined, dried (Na_2SO_4), filtered, and concentrated at reduced pressure, to afford the alkylated pyrazoles (**11**–**13**) as inseparable mixture of N^1 and N^2 isomers (ratio approximately 1:4). This mixture of N^1- and N^2-substituted-4-cyano-5-amino pyrazoles (**11**–**13**) was then dissolved in diphenyl ether (50 mL) and 2-furoic acid hydrazide (13 mmol) was added. The mixture was heated at 260 °C using a Dean–Stark for the azeotropic elimination of water produced in the reaction. After 2.5 h, the mixture was poured onto hexane (300 mL) and cooled. The precipitate of crude pyrazole-triazole derivatives (**14**–**16**) was filtered off and utilized for the next step without further purifications. The crude residue was dissolved in *N*-methyl pyrrolidone (40 mL), cyanamide (60 mmol) and *p*-toluen sulfonic acid (15 mmol) were added, and the mixture was heated at 160 °C for 4 h. Cyanamide (60 mmol) was added again and the solution was heated overnight. Then the solution was diluted with EtOAc (80 mL) and the precipitate (excess of cyanamide) was filtered off; the filtrate was concentrated under reduced pressure and washed with water (3× 30 mL). The organic layer was dried (Na_2SO_4) and evaporated under vacuum. The residue was purified by flash chromatography (EtOAc/light petroleum 3:7) for obtaining the major product (N^8 alkylated) (**17**–**19**) which was obtained in a good overall yield.

3.1.2.1. 5-Amino-8-(4-methyl-pent-1-yl)-2-(2-furyl)-pyrazolo[4,3-*e*]1,2,4-triazolo[1,5-*c*]pyrimidine (17). Yield 65%; pale yellow; mp (EtOAc–light petroleum) 163 °C; IR (KBr): 3420–2950, 1670, 1650, 1620, 1550, 1450 cm^{-1}; ^{1}H NMR (DMSO-d_6) δ: 0.91 (d, 6H, J = 7); 1.10–1.27 (m, 2H); 1.54–1.57 (m, 1H); 1.95–1.98 (m, 2H); 4.31 (t, 2H, J = 7); 5.93 (br s, 2H); 6.62 (dd, 1H, J = 2, J = 4); 7.29 (d, 1H, J = 4); 7.62 (d, 1H, J = 2); 8.15 (s, 1H). Anal. ($C_{16}H_{19}N_7O$) C, H, N.

3.1.2.2. 5-Amino-8-*n*-pentyl-2(2-furyl)-pyrazolo[4,3-*e*]-1,2,4-triazolo[1,5-*c*]pyrimidine (18). Yield 58%; pale yellow solid; mp (EtOAc–light petroleum) 90–92 °C; IR (KBr): 3445–2960, 1675, 1650, 1615, 1555, 1450 cm^{-1}; ^{1}H NMR (DMSO-d_6) δ: 0.91 (t, 3H, J = 7); 1.27–1.49 (m, 4H); 1.71–1.89 (m, 2H); 4.18 (q, 2H, J = 7); 6.21 (br s, 2H); 6.65 (dd, 1H, J = 2, J = 4); 7.16 (d, 1H,

$J = 4$); 7.73 (d, 1H, $J = 2$); 8.24 (s, 1H). Anal. ($C_{15}H_{15}N_7O$) C, H, N.

3.1.2.3. 5-Amino-8-*n*-hexyl-2(2-furyl)-pyrazolo[4,3-*e*]-1,2,4-triazolo[1,5-*c*]pyrimidine (19). Yield 63%; pale yellow solid; mp (EtOAc–light petroleum) 115–118 °C; IR (KBr): 3435–2970, 1665, 1640, 1615, 1550, 1470 cm^{-1}; ^1H NMR (DMSO-d_6) δ: 0.92 (t, 2H, $J = 7$); 1.09–1.32 (m, 4H); 1.65–1.80 (m, 2H); 1.91–2.05 (m, 2H); 4.18 (q, 2H, $J = 7$); 6.11 (br s, 2H); 6.65 (dd, 1H, $J = 2$, $J = 4$); 7.18 (d, 1H, $J = 4$); 7.81 (d, 1H, $J = 2$); 8.11 (s, 1H). Anal. ($C_{16}H_{17}N_7O$) C, H, N.

3.1.3. General procedure for the preparation of 5-[[(substituted)amino]carbonyl]amino-8-alkyl-2-(2-furyl)-pyrazolo[4,3-*e*]1,2,4-triazolo[1,5-*c*]pyrimidines (1–9). Amino compound (**17**–**22**) (10 mmol) was dissolved in freshly distilled dioxane (15 mL) and the appropriate isocyanate (**23**–**29**) (13 mmol) was added. The mixture was refluxed under argon for 18 h. Then the solvent was removed under reduced pressure and the residue was purified by flash chromatography (EtOAc–light petroleum 7:3) to afford the desired compounds **1**–**9**.

3.1.3.1. 4-[3-(2-Furan-2-yl-8-cyclohexylmethyl-8*H*-pyrazolo[4,3-*e*][1,2,4]triazolo[1,5-*c*]pyrimidin-5-yl)-ureido]-phenylacetone (1). Yield 88%; white solid; mp (EtOAc–light petroleum) 198 °C; IR (KBr): 3255–2960, 1710, 1678, 1610, 1600, 1530 cm^{-1}; ^1H NMR ($CDCl_3$) δ: 1.01–1.41 (m, 3H); 1.55–1.98 (m, 8H); 2.11 (s, 3H); 3.62 (s, 3H); 4.12 (d, 2H, $J = 8$); 6.62 (dd, 1H, $J = 2$, $J = 4$); 7.18 (d, 2H, $J = 9$); 7.25 (d, 1H, $J = 4$); 7.62 (d, 2H, $J = 9$); 7.71 (d, 1H, $J = 2$); 8.22 (s, 1H); 8.62 (br s, 1H); 11.13 (br s, 1H). Anal. ($C_{27}H_{28}N_8O_3$) C, H, N.

3.1.3.2. 5-[[(1-Methyl-prop-1-yl)amino]carbonyl]amino-8-ethyl-2-(2-furyl)-pyrazolo[4,3-*e*]1,2,4-triazolo[1,5-*c*]-pyrimidine (2). Yield 78%; pale yellow solid; mp (EtOAc–light petroleum) 167 °C; IR (KBr): 3245–2975, 1675, 1615, 1605, 1510 cm^{-1}; ^1H NMR ($CDCl_3$) δ: 1.01 (t, 3H, $J = 7$); 1.12 (d, 3H, $J = 7$); 1.21 (t, 3H, $J = 7$); 1.45–1.67 (m, 2H); 3.85–4.02 (m, 1H); 4.21 (q, 2H, $J = 7$); 6.61 (dd, 1H, $J = 2$, $J = 4$); 7.26 (d, 1H, $J = 4$); 7.96 (d, 1H, $J = 2$); 8.12 (s, 1H); 8.43 (br s, 1H); 8.98 (br s, 1H). Anal. ($C_{17}H_{20}N_8O_2$) C, H, N.

3.1.3.3. 4-[3-(2-Furan-2-yl-8-(4-methyl-pent-1-yl)-8*H*-pyrazolo[4,3-*e*][1,2,4]triazolo[1,5-c]pyrimidin-5-yl)-ureido]-phenylacetic acid methyl ester (3). Yield 78%; white solid; mp (EtOAc–light petroleum) 168 °C; IR (KBr): 3255–2970, 1720, 1675, 1615, 1600, 1510 cm^{-1}; ^1H NMR ($CDCl_3$) δ: 0.92 (d, 6H, $J = 7$); 1.01–1.15 (m, 2H); 1.21–1.37 (m, 1H); 1.82–1.99 (m, 2H); 3.12 (s, 2H); 3.62 (s, 3H); 4.19 (q, 2H, $J = 7$); 6.72 (dd, 1H, $J = 2$, $J = 4$); 7.17 (d, 2H, $J = 9$); 7.26 (d, 1H, $J = 4$); 7.51 (d, 2H, $J = 9$); 7.76 (d, 1H, $J = 2$); 8.05 (s, 1H); 8.81 (br s, 1H); 10.63 (br s, 1H). Anal. ($C_{26}H_{28}N_8O_4$) C, H, N.

3.1.3.4. 5-[[(Ethyl)amino]carbonyl]amino-8-*n*-propyl-2-(2-furyl)-pyrazolo[4,3-*e*]1,2,4-triazolo[1,5-*c*]pyrimidine (4). Yield 67%; white solid; mp (EtOAc–light petroleum) 193 °C; IR (KBr): 3255–2975, 1670, 1615, 1600, 1525 cm^{-1}; ^1H NMR ($CDCl_3$) δ: 1.01 (t, 3H, $J = 7$); 1.19 (t, 3H, $J = 7$); 2.01–2.16 (m, 2H); 3.20–3.35 (m, 2H); 4.18 (t, 2H, $J = 7$); 6.61 (dd, 1H, $J = 2$, $J = 4$); 7.21 (d, 1H, $J = 4$); 7.70 (d, 1H, $J = 2$); 8.11 (s, 1H); 8.30 (br s, 1H); 9.01 (br t, 1H). Anal. ($C_{16}H_{18}N_8O_2$) C, H, N.

3.1.3.5. 5-[[(Cyclohexylmethyl)amino]carbonyl]amino-8-*n*-propyl-2-(2-furyl)-pyrazolo[4,3-*e*]1,2,4-triazolo-[1,5-*c*]-pyrimidine (5). Yield 93%; white solid; mp (EtOAc–light petroleum) 165 °C; IR (KBr): 3250–2955, 1665, 1625, 1605, 1510 cm^{-1}; ^1H NMR ($CDCl_3$) δ: 0.79–1.05 (m, 9H); 1.18–1.59 (m, 5H); 1.94–2.01(m, 2H); 3.09–3.15 (m, 2H); 4.12 (t, 2H, $J = 7$); 6.59 (dd, 1H, $J = 2$, $J = 4$); 7.11 (d, 1H, $J = 4$); 7.64 (d, 1H, $J = 2$); 8.03 (s, 1H); 8.18 (br s, 1H); 8.89 (br s, 1H). Anal. ($C_{21}H_{26}N_8O_2$) C, H, N.

3.1.3.6. 4-[3-(2-Furan-2-yl-8-cyclohexylmethyl-8*H*-pyrazolo[4,3-*e*][1,2,4]triazolo[1,5-*c*]pyrimidin-5-yl)-ureido]-phenylacetic acid methyl ester (6). Yield 70%; pale yellow solid; mp (EtOAc–light petroleum) 158 °C; IR (KBr): 3230–2955, 1720, 1675, 1615, 1600, 1520 cm^{-1}; ^1H NMR ($CDCl_3$) δ: 0.99–1.21 (m, 6H); 1.62–1.81 (m, 5H); 3.59 (s, 2H); 3.71 (s, 3H); 4.21 (d, 2H, $J = 6$); 6.63 (dd, 1H, $J = 2$, $J = 4$); 7.21 (d, 2H, $J = 9$); 7.25 (d, 1H, $J = 4$); 7.64 (d, 2H, $J = 7$); 7.67 (d, 1H, $J = 2$); 8.18 (s, 1H); 8.61 (br s, 1H); 11.09 (br s, 1H). Anal. ($C_{27}H_{28}N_8O_4$) C, H, N.

3.1.3.7. 4-[3-(2-Furan-2-yl-8-*n*-pentyl-8*H*-pyrazolo[4,3-*e*][1,2,4]triazolo[1,5-*c*]pyrimidin-5-yl)-ureido]-phenylacetic acid ethyl ester (7). Yield 65%; pale yellow solid; mp (EtOAc–light petroleum) 170 °C; IR (KBr): 3245–2955, 1715, 1675, 1615, 1600, 1525 cm^{-1}; ^1H NMR ($CDCl_3$) δ: 0.97 (t, 3H, $J = 7$); 1.15 (t, 3H, $J = 7$); 1.18–1.24 (m, 4H); 1.98–2.15 (m, 2H); 3.61 (s, 3H); 4.19 (q, 2H, $J = 7$); 4.41 (t, 2H, $J = 7$); 6.61 (dd, 1H, $J = 2$, $J = 4$); 7.22 (d, 2H, $J = 9$); 7.25 (d, 1H, $J = 4$); 7.61 (d, 2H, $J = 9$); 7.64 (d, 1H, $J = 2$); 8.19 (s, 1H); 8.61 (br s, 1H); 11.09 (br s, 1H). Anal. ($C_{26}H_{28}N_8O_4$) C, H, N.

3.1.3.8. 5-[[(1-Methyl-prop-1-yl)amino]carbonyl]amino-8-*n*-hexyl-2-(2-furyl)-pyrazolo[4,3-*e*]1,2,4-triazolo[1,5-*c*]-pyrimidine (8). Yield 88%; white solid; mp (EtOAc–light petroleum) 115 °C; IR (KBr): 3240–2965, 1670, 1615, 1565 cm^{-1}; ^1H NMR ($CDCl_3$) δ: 0.85–1.01 (m, 9H); 1.21–1.40 (m, 4H); 1.58–1.67 (m, 4H); 1.91–2.18 (m, 2H); 3.97–4.09 (m, 1H); 4.39 (t, 2H, $J = 7$); 6.62 (dd, 1H, $J = 2$, $J = 4$); 7.23 (d, 1H, $J = 4$); 7.65 (d, 1H, $J = 2$); 8.21 (s, 1H); 8.45 (br s, 1H); 8.82 (br s, 1H). Anal. ($C_{21}H_{28}N_8O_2$) C, H, N.

3.1.3.9. 5-[[(*n*-Hexyl)amino]carbonyl]amino-8-(4-tolyl)-2-(2-furyl)-pyrazolo[4,3-*e*]1,2,4-triazolo[1,5-*c*]pyrimidine (9). Yield 93%; pale yellow solid; mp (EtOAc–light petroleum) 184 °C; IR (KBr): 3250–2970, 1673, 1610, 1545 cm^{-1}; ^1H NMR ($CDCl_3$) δ: 0.97 (t, 3H, $J = 7$); 1.21–1.39 (m, 6H); 1.99–2.15 (m, 2H); 2.19 (s, 3H); 4.40 (t, 2H, $J = 7$); 6.61 (dd, 1H, $J = 2$, $J = 4$); 7.17 (d, 2H, $J = 9$); 7.22 (d, 1H, $J = 4$); 7.58 (d, 2H, $J = 9$); 7.69 (d, 1H, $J = 2$); 8.21 (s, 1H); 8.60 (br s, 1H); 11.01 (br s, 1H). Anal. ($C_{24}H_{26}N_8O_2$) C, H, N.

4. Biology

All pharmacological methods followed the procedures as described earlier.[24] In brief, membranes for radioligand binding were prepared from CHO cells stably transfected with human adenosine receptor subtypes in a two-step procedure. In a first low-speed step (1000*g*), cell fragments and nuclei were removed. The crude membrane fraction was sedimented from the supernatant at 100,000*g*. The membrane pellet was resuspended in the buffer used for the respective binding experiments, frozen in liquid nitrogen, and stored at −80 °C. For the measurement of adenylyl cyclase activity, only one high speed centrifugation of the homogenate was used. The resulting crude membrane pellet was resuspended in 50 mM Tris–HCl, pH 7.4, and immediately used for the cyclase assay.

For radioligand binding at A_1 adenosine receptors 1 nM [^{3}H]CCPA was used, whereas 30 and 10 nM [^{3}H]NECA were used for A_{2A} and A_3 receptors, respectively. Non-specific binding of [^{3}H]CCPA was determined in the presence of 1 mM theophylline, in the case of [^{3}H]NECA 100 μM R-PIA was used. K_i-values from competition experiments were calculated with the program SCTFIT.[25]

Radioligand binding at A_{2B} adenosine receptors is problematic as no high-affinity ligand is available for this subtype. Therefore, inhibition of NECA-stimulated adenylyl cyclase activity was determined as a measurement of affinity of compounds. EC_{50}-values from these experiments were converted to K_i-values with the Cheng and Prusoff equation.[26]

5. Computational methodologies

All modeling and 3D-QSAR studies were carried out on a 10 CPU (PIV-3.0GHZ and AMD64) linux cluster running under OpenMosix architecture.[27] Homology modeling, energy calculation, and docking studies have been done using Molecular Operating Environment (MOE, version 2004.03) suite.[28]

Autocorrelation MEP studies have been done using ADRIANA (version 1.0) suite.[29] All PLS analyses have been carried out using 'The Unscrambler statistical software.[30]

5.1. Virtual library construction

Our pyrazolo-triazolo-pyrimidine focused library has been built up using the CombiGen module of MOE suite.[28] CombiGen method enumerates a virtual library of all possible products that are combinatorially generated from a set of molecular fragments. The virtual library is constructed by functionalizing the central molecular moiety called scaffold. Both monofunctionalized and bifunctionalized as well as symmetric substitutions are supported, and substitution through higher-order bonds is also allowed. Conformer generation and best conformer selection have been carried out using standard parameters of Corina. All finally used compounds are in their ionized form at a physiological pH. Corina is an integral part of the ADRIANA QSAR suite.[29]

5.2. Molecular electrostatic potential (MEP) calculation

In the present work, MEPs derive from a classical point charge model: the electrostatic potential for each molecule is obtained by moving a unit positive point charge across the van der Waals surface and it is calculated at various points j on this surface by the following equation:[19,20]

$$V_j = \sum_i^{\text{atoms}} \frac{q_i}{r_{ji}},$$

where q_i represents the partial charge of each atom i and r_{ji} is the distance between points j and atom i. Starting from the 3D model of a molecule and its partial atomic charges, the electrostatic potential or another appropriate property is calculated for points on the molecular surface. Partial atomic charges were calculated by the PEOE method[31] and its extension to conjugated systems[32] implemented by Petra module of Adriana suite.[29] Connolly's solvent accessible surface with a solvent radius of 2.0 Å has been used to project the corresponding MEP. For the pyrazolo-triazolo-pyrimidine derivative (**1**) (shown in Table 1), about 3500 points are obtained which are characterized by their Cartesian coordinates and the value of the electrostatic potential. After applying the autocorrelation function, the autocorrelation vector is obtained. Connolly's solvent accessible surface and the corresponding MEP have been calculated by Surface module of Adriana.[29]

5.3. Autocorrelation vector

The first application of these vectors as molecular descriptors has been published by Moreau and Broto,[33,34] who applied the classical mathematical notion of an autocorrelation function to the topology of molecular structures. The autocorrelation vector is presented as an intrinsic descriptor of the distribution of an atomic property along the molecular graph. Each component of the autocorrelation vector is calculated as follows:

$$A(d) = \sum_{ij} p_i p_j,$$

where A is the autocorrelation coefficient referring to atom pairs ij, p_i is the atomic property, and d is the ij topological distance.

Starting from this concept a new 3D descriptor has been introduced which is based on the autocorrelation of properties at distinct points on the molecular surface.[19,20] The different components of the autocorrelation vector are derived in this way:

$$A(d_{\text{lower}}, d_{\text{upper}}) = 1/L \sum p_i p_j (d_{\text{lower}} < d_{ij} < d_{\text{upper}}),$$

where the ij distance d belongs to the d_{lower}, d_{upper} interval and L is number of distances in the same interval.

The application of this concept made possible to compare different molecular properties, as this 3D descriptor represents a compressed expression of the distribution of the property p on the molecular surface.[19,20] The parameters for the calculation of the autocorrelation coefficient are the following: $d_{lower} = 1$ Å; $d_{upper} = 13$ Å; $L = 12$; point density = 10 points/Å^2; *vdW* radius reduction factor = 1.000. All parameters have been changed in a various way to see if it was possible to improve the model capability, but non-significant results were derived. Considering distances from 1 to 13 Å, with a step width of 1 Å, twelve autocorrelation coefficients are calculated. This transformation produces a unique fingerprint of each molecule under consideration. Autocorrelation vector has been calculated by Surface module of Adriana.[29]

5.4. Partial least squares (PLS) analysis

All PLS analyses have been carried out using 'The Unscrambler statistical software.[30]

5.5. Homology model of the resting state of human A_3 receptor

Based on the assumption that GPCRs share similar TM boundaries and overall topology,[35] a homology model of the human A_3 receptor was constructed. First, the amino acid sequences of TM helices of the resting state A_3 receptor were aligned with those of bovine rhodopsin, guided by the highly conserved amino acid residues, including the DRY motif (D3.49, R3.50, and Y3.51) and three Pro residues (P4.60, P6.50, and P7.50) in the TM segments of GPCRs. The same boundaries were applied for the TM helices of the A_3 receptor as were identified from the X-ray crystal structure for the corresponding sequences of bovine rhodopsin,[36] the C_α coordinates which were used to construct the seven TM helices for the human A_3 receptor. The loop domains of the human A_3 receptor were constructed by the loop search method implemented in MOE. In particular, loops are modeled first, in random order. For each loop, a contact energy function analyzes the list of candidates collected in the segment searching stage, taking into account all atoms already modeled and any atom specified by the user as belonging to the model environment. These energies are then used to make a Boltzmann-weighted choice from the candidates, the coordinates of which are then copied to the model. Any missing sidechain atoms are modeled using the same procedure. Sidechains belonging to residues whose backbone coordinates were copied from a template are modeled first, followed by sidechains of modeled loops. Outgaps and their sidechains are modeled last. Special caution had to be given to the second extracellular (E2) loop, which has been described in bovine rhodopsin to fold back over transmembrane helices,[36] and, therefore, it limits the size of the active site. Hence, amino acids of this loop could be involved in direct interactions with the ligands. The presence of a disulfide bridge between cysteines in TM3 and E2 might be the driving force to this peculiar fold of the E2 loop. Since this covalent link is conserved in all receptors modeled in the current study, the E2 loop was modeled using a rhodopsin-like constrained geometry around the E2–TM3 disulfide bridge. After the heavy atoms were modeled, all hydrogen atoms were added, and the protein coordinates were then minimized with MOE using the AMBER94 force field.[37] The minimizations were carried out by 1000 steps of steepest descent followed by conjugate gradient minimization until the rms gradient of the potential energy was less than 0.1 kcal/mol Å.

5.6. Molecular docking (multi-docking) of the human A_3 receptor antagonists

All the newly synthetized antagonist structures were docked into the hypothetical TM binding site by using the MULTIDOCK docking program, that is part of the MOE suite. Conformational samplings were conducted within a user-specified 3D docking box, using Tabù Search protocol[38] and MMFF94 force field.[39] MOE-Dock performs a user-specified number of independent docking runs (50 in our specific case) and wrote the resulting conformations and their energies in a molecular database file. The resulting docked complexes were subjected to MMFF94 energy minimization until the rms of conjugate gradient was <0.1 kcal/mol Å^{-1}. Charges for the ligands were imported directly from the MMFF94 force field.

The interaction energy values were calculated as follows: $\Delta E_{binding} = E_{complex} - (E_{ligand} + E_{receptor})$. These energies are not rigorous thermodynamic quantities, but can only be used to compare the relative stabilities of the complexes. Therefore, these interaction energy values cannot be used to calculate binding affinities since changes in entropy and solvation effects are not taken into account.

Acknowledgments

We thank Molecular Network GmbH (Erlangen, Germany) for the assistance in using ADRIANA modeling suite. The molecular modeling work coordinated by S.M. has been carried out with financial supports of the Italian Ministry for University and Research (MIUR), Rome, Italy, and of the University of Padova, Padova, Italy. S.M. is also really grateful to Chemical Computing Group for the scientific and technical partnership.

Supplementary data

Supporting information available: Tables listing elementary analysis of all newly synthetized compounds and compounds predicted as more active (~100 molecules) with a spectrum of predicted activity in the range of 0.1–4.0 nM. Supplementary data associated with this article can be found, in the online version, at doi:10.1016/j.bmc.2006.03.010.

References and notes

1. Schneider, G.; Fechner, U. *Nat. Rev. Drug Disc.* **2005**, *4*, 649–663.
2. Geysen, H. M.; Schoenen, F.; Wagner, D.; Wagner, R. *Nat. Rev. Drug Disc.* **2003**, *2*, 222–230.
3. Shoichet, B. K. *Nature* **2004**, *432*, 862–865.
4. Langer, T.; Wolber, G. *Pure Appl. Chem.* **2004**, *76*, 991–996.
5. Jain, A. N. *Curr. Opin. Drug Discov. Devel.* **2004**, *7*, 396–403.
6. Stahura, F. L.; Bajorath, J. *Curr. Pharm. Des.* **2005**, *11*, 1189–1202.
7. Bissantz, C.; Schalon, C.; Guba, W.; Stahl, M. *Proteins* **2005**, *61*, 938–952.
8. Evers, A.; Hessler, G.; Matter, H.; Klabunde, T. *J. Med. Chem.* **2005**, *48*, 5448–5465.
9. Matter, H.; Baringhaus, K. H.; Naumann, T.; Klabunde, T.; Pirard, B. *Comb. Chem. High Throughput Screening* **2001**, *4*, 453–475.
10. Ajay, S. *Curr. Top. Med. Chem.* **2002**, *2*, 1273–1286.
11. Lowrie, J. F.; Delisle, R. K.; Hobbs, D. W.; Diller, D. J. *Comb. Chem. High Throughput Screening* **2004**, *7*, 495–510.
12. Moro, S.; Bacilieri, M.; Ferrari, C.; Spalluto, G. *Curr. Drug Discov. Tech.* **2005**, *2*, 13–21.
13. Moro, S.; Bacilieri, M.; Cacciari, B.; Spalluto, G. *J. Med. Chem.* **2005**, *48*, 5698–5704.
14. Fredholm, B. B.; IJzerman, A. P.; Jacobson, K. A.; Klotz, K. N.; Linden, J. *Pharmacol. Rev.* **2001**, *53*, 527–552.
15. Moro, S.; Deflorian, F.; Spalluto, G.; Pastorin, G.; Cacciari, B., et al. *Chem. Commun. (Camb.)* **2003**, *24*, 2949–2956.
16. Moro, S.; Spalluto, G.; Jacobson, K. A. *Trends Pharmacol. Sci.* **2005**, *26*, 44–51.
17. Moro, S.; Braiuca, P.; Deflorian, F.; Ferrari, C.; Pastorin, G.; Cacciari, B.; Baraldi, P. G.; Varani, K.; Borea, P. A.; Spalluto, G. *J. Med. Chem.* **2005**, *48*, 152–162.
18. Baraldi, P. G.; Fruttarolo, F.; Tabrizi, M. A.; Preti, D.; Romagnoli, R.; El-Kashef, H.; Moorman, A.; Varani, K.; Gessi, S.; Merighi, S.; Borea, P. A. *J. Med. Chem.* **2003**, *46*, 1229–1241.
19. Gasteiger, J.; Li, X.; Rudolph, C.; Sadowsky, J.; Zupan, J. *J. Am. Chem. Soc.* **1994**, *116*, 4608–4620.
20. Wagener, M.; Sadowsky, J.; Gasteiger, J. *J. Am. Chem. Soc.* **1995**, *117*, 7769–7775.
21. Gatta, F.; Del Giudice, M. R.; Borioni, A.; Borea, P. A.; Dionisotti, S.; Ongini, E. *Eur. J. Med. Chem.* **1993**, *28*, 569–577.
22. Baraldi, P. G.; Cacciari, B.; Romagnoli, R.; Spalluto, G.; Moro, S.; Klotz, K. N.; Leung, E.; Varani, K.; Gessi, S.; Merighi, S.; Borea, P. A. *J. Med. Chem.* **2000**, *43*, 4768–4780.
23. Kurita, K.; Iwakura, Y. *Org. Synth. Coll. Vol. VI* **1988**, 715–718.
24. Klotz, K. N.; Hessling, J.; Hegler, J.; Owman, C.; Kull, B.; Fredholm, B. B.; Lohse, M. J. *Naunyn-Schmiedeberg's Arch. Pharmacol.* **1998**, *357*, 1–9.
25. De Lean, A.; Hancock, A. A.; Lefkowitz, R. J. *Mol. Pharmacol.* **1982**, *21*, 5–16.
26. Cheng, Y.-C.; Prusoff, W. H. *Biochem. Pharmacol.* **1973**, *22*, 3099–3108.
27. OpenMosix: http://www.openMosix.org, 2004.
28. Molecular Operating Environment (MOE 2004.03), C.C.G., Inc., 1255 University St., Suite 1600, Montreal, Que., Canada H3B 3X3.
29. ADRIANA; Molecular Networks GmbH: Erlangen, Germany, 2003.
30. 'The Unscramble' (version 9.0), CAMO Process AS, Oslo, Norway, 2003.
31. Gasteiger, J.; Marsili, M. *Tetrahedron* **1980**, *36*, 3219–3228.
32. Gasteiger, J.; Saller, H. *Angew. Chem.* **1985**, *97*, 699–701.
33. Moreau, G.; Broto, P. *Nouv. J. Chim.* **1980**, *4*, 359–360.
34. Moreau, G.; Broto, P. *Nouv. J. Chim.* **1980**, *4*, 757–764.
35. Saunders, J. *Drug Discovery Today* **2001**, *6*, 288–289.
36. Palczewski, K.; Kumasaka, T.; Hori, T.; Behnke, C. A.; Motoshima, H., et al. *Science* **2000**, *289*, 739–745.
37. Cornell, W. D. C. P.; Bayly, C. I.; Gould, I. R.; Merz, K. M.; Ferguson, D. M.; Spellmeyer, D. C.; Fox, T.; Caldwell, J. W.; Kollman, P. A. A. *J. Am. Chem. Soc.* **1995**, *117*, 5179–5196.
38. Baxter, C. A.; Murray, C. W.; Clark, D. E.; Westhead, D. R.; Eldridge, M. D. *Proteins: Struct., Funct. Genet.* **1998**, *33*, 367–382.
39. Halgren, T. *J. Comput. Chem.* **1996**, *17*, 490–519.